Journal of Organometallic Chemistry, 426 (1992) 195–212
Elsevier Sequoia S.A., Lausanne
JOM 22319

Electrochemistry and bonding in biscyclopentadienyl complexes of molybdenum, tungsten, and niobium with *o*-phenanthroline and bipyridine. Crystal and molecular structures of $[Nb(\eta^5\text{-}C_5H_5)_2(bpy)][PF_6]_2$ and $[M(\eta^5\text{-}C_5H_5)_2(o\text{-phen})][PF_6]_2$ (M = Mo or W)

Maria J. Calhorda, Maria A.A.F. de C.T. Carrondo, Andreas Bram, Pia N. Olsen

Centro de Tecnologia Química e Biológica, R. da Quinta Grande 6, 2780 Oeiras and I.S.T., Av. Rovisco Pais, 1096 Lisboa Codex (Portugal)

Alberto R. Dias, Ana M. Freitas, M. Helena Garcia and M. Fátima M. Piedade

Centro de Química Estrutural, Complexo I, I.S.T., Av. Rovisco Pais, 1096 Lisboa Codex (Portugal)

(Received August 8, 1991)

Abstract

The electrochemical behaviour of the new Nb^{IV} derivatives $[Nb(\eta^5\text{-}C_5H_5)_2(L\text{–}L)][PF_6]_2$ where L–L = 2,2′-bipyridyl or *o*-phenanthroline and of the molybdenum(IV) and tungsten(IV) analogues was investigated and the reduction of the coordinated ligand was observed along with the redox processes based on the metal.

The structure of the new $[Nb(\eta^5\text{-}C_5H_5)_2(bpy)][PF_6]_2$ (**1**) and of the known related compounds $[Mo(\eta^5\text{-}C_5H_5)_2(o\text{-phen})][PF_6]_2$ (**2**) and $[W(\eta^5\text{-}C_5H_5)_2(o\text{-phen})][PF_6]_2$ (**3**) have been characterized by single crystal X-ray diffraction studies. The Mo and the W complexes are isostructural, while the Nb complex crystallizes in a slightly different monoclinic cell. In complex **1** the Nb–N bond distances are 2.226(6) and 2.218(6) Å and the bond angle is 72.6(3)°, while in complex **2**, Mo–N bond distances are 2.193(7) and 2.186(7) Å and the N–Mo–N bond angle is 74.7(3)° and in complex **3**, W–N bond distances are 2.181(11) and 2.179(9) Å and the N–W–N bond angle is 74.7(4)°.

An extended-Hückel molecular-orbital study of the bonding of these complexes showed the absence of back donation to the low-energy, empty orbitals of the nitrogen ligand.

Introduction

Biscyclopentadienyl complexes of transition metals, such as molybdenum, tungsten and titanium, containing neutral bidentate ligands with nitrogen donor atoms

Correspondence to: Dr. M.J. Calhorda, Centro de Tecnologia Química e Biológica, R. da Quinta Grande 6, Portugal.

have been known for a number of years [1]. Whereas the titanium(III, IV) derivatives were not subject to further studies, the reactivity of the molybdenum and tungsten dications with *o*-phenanthroline (*o*-phen) and bipyridine (bpy) ligands was investigated both chemically [1] and photochemically [2], in order to compare them with those of neutral bidentate phosphorus ligands [3] and of monodentate nitrogen ligands [1,2,4]. These complexes proved to be inert towards photochemically induced ligand substitution, for instance, and nucleophilic attack led to their decomposition. In the following study, the crystal and molecular structures of the new $[Nb(\eta^5\text{-}C_5H_5)_2(bpy)][PF_6]_2$ complex **1**, ($\eta^5\text{-}C_5H_5 = Cp$), as well as of the molybdenum and tungsten derivatives, $[Mo(\eta^5\text{-}C_5H_5)_2(o\text{-phen})][PF_6]_2$ (**2**), and $[W(\eta^5\text{-}C_5H_5)_2(o\text{-phen})][PF_6]_2$ (**3**), are described. The electrochemical behaviour of these and other related complexes was investigated and an extended-Hückel molecular-orbital study [5] was undertaken in order to clarify the experimental results.

Results and discussion

Chemical studies

The complex $[NbCp_2Cl_2]$ reacts with bipyridine or *o*-phenanthroline in the presence of $Tl[PF_6]$ to give red-orange crystals of the complexes $[NbCp_2(bpy)][PF_6]_2$ (**1**) or $[NbCp_2(o\text{-phen})][PF_6]_2$ (**4**), after several hours at room temperature, or *ca.* 30 min at reflux. A higher yield (*ca.* 50%) was obtained when the reaction was carried out at room temperature. A white impurity, which made isolation of the orange analytically pure product difficult, was sometimes randomly formed during the reaction. This problem was mentioned by other authors as occurring during the synthesis of some related biscyclopentadienyl niobium compounds [6].

The Nb^{IV} complexes are soluble in acetone and acetonitrile and insoluble in dichloromethane and ether. In the solid state they are fairly stable towards oxidation by air. Characteristic IR bands confirm the presence of both the $NbCp_2$ (*ca.* 3100 cm^{-1}) fragment and the PF_6^- cation (840 and 560 cm^{-1}) as well as the coordinated bpy (1605, 770, 730, 420 cm^{-1}) or *o*-phen (1635, 1605, 1585, 1520, 1430 cm^{-1}). The complexes $[MoCp_2(o\text{-phen})][PF_6]_2$ (**2**) and $[WCp_2(o\text{-phen})][PF_6]_2$ (**3**) were prepared following published procedures [1].

Electrochemical studies

Selected data for compounds **1–4** and the related $[WCp_2(bpy)][PF_6]_2$ (**5**) are collected in Table 1.

The cyclic voltammograms of the Nb^{IV} compound, $[NbCp_2(bpy)][PF_6]_2$ (**1**), in acetonitrile solution between the solvent limits (*ca.* −1.8 and 1.6 V) exhibited two reversible redox processes at $E_{p/2} = -0.305$ and −1.350 V, at scan rates between 20 and 500 mV/s (Fig. 1).

For both processes, a plot of i_a against the square root of the scan speed was linear, as expected for diffusion-controlled electrode processes. The average of the anodic and cathodic peak potentials was independent of the scan speed and the separation of these waves, ΔE_p, was 70 and 60 mV respectively (see Table 1).

Analyses of cyclic voltammograms, such as the one shown in Fig. 1, lead us to assign the first redox process at $E_{p/2} = -0.305$ mV to the one-electron reduction $Nb^{IV} \rightarrow Nb^{III}$. When the scan was started at 0 V, no cathodic current was

Table 1

Electrochemical data [a]

Compound	E_{pa}	E_{pc}	$E_{pa} - E_{pc}$ (mV)	$E_{p/2}$ (V)
$[NbCp_2(bpy)]^{2+}$ (1)	−0.270	−0.340	70	−0.305
	−1.320	−1.380	60	−1.350
$[MoCp_2(o\text{-phen})]^{2+}$ (2)	1.680	1.580	110	1.625
	−0.920	-		
	−1.350	-		
$[WCp_2(o\text{-phen})]^{2+}$ (3)	1.480	1.420	60	1.450
	−0.870	-		
	−1.400	-		
$[NbCp_2(o\text{-phen})]^{2+}$ (4)	−0.340	−0.280	65	−0.310
	−1.340	-		
	-	−0.890		
$[WCp_2(bpy)]^{2+}$ (5) [b]	1.80	1.10	70	1.46

[a] Experimental conditions: Electrochemical data were obtained in CH_3CN containing 0.1 $Bu_4N[PF_6]$ and are referred to a calomel electrode saturated with KCl. The sweep rate was 200 mV/s and I_a/I_c for reversible waves was approximately 1. [b] Ref. 10.

observed. If the scan started at −0.8 V, however, an anodic current was observed corresponding to the reoxidation of Nb^{III} species. The second redox process at $E_{p/2} = -1.350$ V was assigned to the redox-active coordinated bipyridine (free molecule: $E_{p/2}$ *ca.* −2.1 V) [7]. Such a shift towards less negative potentials has been reported for several families of compounds containing this ligand [8]. The explanation has been based on a stabilization of the reduced form of the ligand by the central field of the metal atom which carries a positive charge. The stabilization of the π-orbitals of the ligand would arise due to the decrease of electron density on the donor atom σ-bonded to the metal.

Cyclic voltammograms for $[NbCp_2(o\text{-phen})][PF_6]_2$ (4) show a reversible redox process at $E_{p/2} = -0.310$ V attributed to the one-electron reduction $Nb^{IV} \rightarrow Nb^{III}$, at approximately the same potential as for the bipyridine analogue. However, the

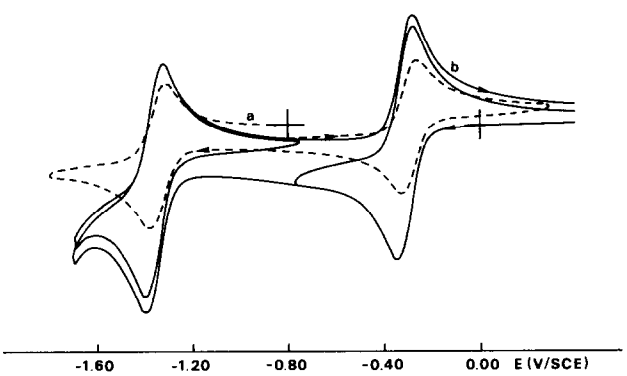

Fig. 1. Cyclic voltammogram of $[Nb(\eta^5\text{-}C_5H_5)_2(bpy)][PF_6]_2$ (1) in CH_3CN containing 0.1 *M* $Bu_4N[PF_6]$ (sweep rate 200 mV/s): (a) sweep started at −0.80 V; (b) sweep started at 0.0 V.

second reduction process, which was there considered to occur on the ligand is now totally irreversible, with a cathodic wave at $E_{pc} = -1.340$ V, and no corresponding anodic wave. In the reverse scan, only a weak anodic wave was found at $E_{pa} = -0.890$ V, probably due to any unidentified decomposition product coming from this irreversible process. The anodic wave corresponding to the first redox process at $E_{p/2} = -0.310$ V was in same position as when the scan potential was reversed before reaching the second irreversible wave. These observations support the inference that these two redox processes are independent of each other, the first being based on the metal centre and the second, at more negative potential, being based on the ligand.

The general features of the cyclic voltammograms for the complexes $[MoCp_2(o\text{-phen})][PF_6]_2$ (**2**) and $[WCp_2(o\text{-phen})][PF_6]_2$ (**3**) in acetonitrile include one redox process at relatively high potentials, $E_{p/2} = 1.63$ and 1.45 V, respectively, assigned to the one-electron oxidation $M^{IV} \rightarrow M^{V}$, and two cathodic waves at approximately -0.900 and -1.400 V, with no corresponding anodic waves. On the reverse scan, after these two irreversible waves two weak anodic peaks were found due to minor decomposition products, but the oxidation wave of $C_5H_5^-$ was not detected (*ca.* -0.2 V *vs* SCE). The reversibility of the one-electron oxidation wave ($\Delta E_p = 60$ mV) for $[WCp_2(o\text{-phen})][PF_6]_2$ was further demonstrated by the linearity of the plot of the peak current *vs* (sweep rate)$^{1/2}$. For $[MoCp_2(o\text{-phen})][PF_6]_2$ (**2**), this oxidation wave at $E_p = 1.63$ V had a quasi-reversible behaviour with $\Delta E_p = 110$ mV and I_a/I_c is $\cong 1$.

As for other related compounds [9], the tungsten *o*-phen derivative has a lower oxidation potential than the molybdenum and the tungsten oxidized species are kinetically the more stable. The oxidative electrochemistry of $[WCp_2(bpy)][PF_6]_2$ (**5**), previously studied in the same experimental conditions [10], shows a similar behaviour with a reversible wave at $E_{p/2} = 1.46$ V, $\Delta E_p = 70$ mV, and $I_a/I_c = 1$. These results, together with those obtained for both Nb-*o*-phen and Nb-bpy compounds, suggest that the chelating ligands *o*-phenanthroline and bipyridine have equivalent roles in terms of electronic effect on the metal centre.

Biscyclopentadienylniobium(IV) neutral derivatives [11] usually exhibit two redox processes, one being $Nb^{IV} \rightarrow Nb^{V}$ and the other $Nb^{IV} \rightarrow Nb^{III}$. In this work only one metal-based redox process was found, leading to surprisingly stable Nb^{III} species.

The absence of the expected $Nb^{IV} \rightarrow Nb^{V}$ oxidation process, which occurs for neutral compounds at relatively low potentials (in our case no waves were observed in the range 0.0–1.6 V), can be explained by the dicationic character of the Nb^{IV} complexes. Only two other dicationic Nb^{IV} niobocene derivatives, $[NbCp'_2L_2]^{2+}$ ($Cp' = C_5H_4SiMe_3$, $L = P(OMe)_3$) [12] and $[NbCp_2(NCMe)_2]^{2+}$ [13], and only a few monocationic analogues [14], have been previously reported. To the best of our knowledge, the results described above constitute the first complete study of the electrochemistry of dicationic niobocene species.

Electrochemical data for related Nb^{III} neutral compounds, such as $[NbCp'_2(SiMe_3)_2ClX]$ ($Cp' = C_5H_4SiMe_3$, $X = PMe_3$, PMe_2Ph, or $P(OMe)_3$), also show quite stable Nb^{III} species, with $E_{p/2}$ in the range -0.85 to -0.35 V (relative to the Nb^{III}/Nb^{IV} redox couple). The authors related the stability of those Nb^{III} complexes to the increase of π-acceptance capability of the ligands [15]. This is probably not the case for our complexes (see later).

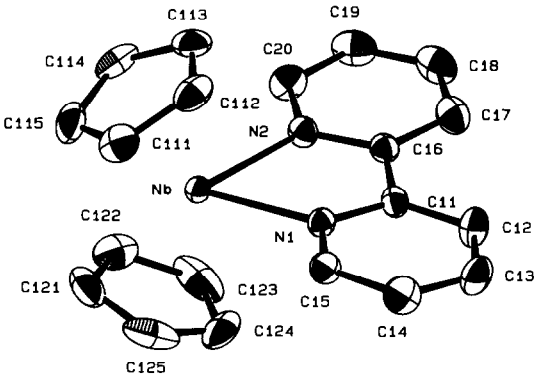

Fig. 2. Molecular structure of $[Nb(\eta^5\text{-}C_5H_5)_2(bpy)][PF_6]_2$ (**1**) with 30% probability thermal ellipsoids showing the atom-labeling scheme (only cation illustrated).

Crystallographic studies

The molecular structures of $[NbCp_2(bpy)][PF_6]_2$ (**1**), $[MoCp_2(o\text{-phen})][PF_6]_2$ (**2**), and $[WCp_2(o\text{-phen})][PF_6]_2$ (**3**) are shown in Figs. 2, 3 and 4, respectively. Selected bond lengths and bond angles for the three complexes are given in Tables 2, 3 and 4, respectively.

The Mo and W complexes are isostructural, whereas the Nb complex crystallizes in a slightly different monoclinic unit cell. All three compounds contain the usual bent metallocene arrangement, with two η^5-cyclopentadienyl rings and the two nitrogen atoms from the aromatic ligand forming a distorted tetrahedral coordination.

The Nb–N bonding distances in **1**, 2.226(6) and 2.218(6) Å, are comparable to 2.165(5) and 2.159(4) Å in $[NbCp_2(NCCH_3)_2][BF_4]_2$ [13], but longer than the values observed in two related binuclear cyclopentadienyl-fulvalene-nitrene complexes, $[Nb_2Cp_2(C_{10}H_8)(\mu\text{-}NAr)_2]$ (average Nb–N distance of 2.04(3) Å) and $[Nb_2Cp_2(C_{10}H_8)(\mu\text{-}NAr)_2][BF_4]$ (average distance of 2.041(6) Å [16]). In these two molecules the geometry of the central planar fragment Nb_2N_2 is a delicate balance of steric and electronic factors; and there is some percentage of double bond

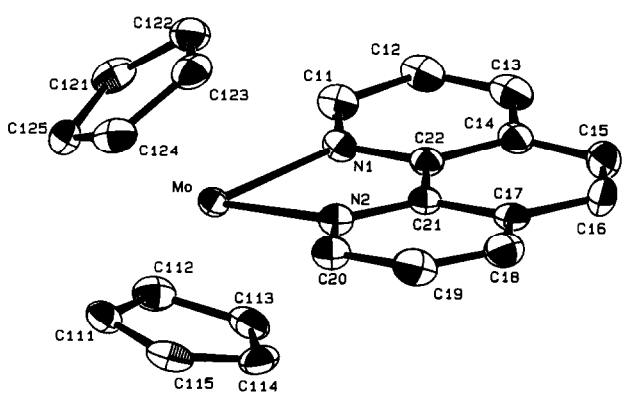

Fig. 3. Molecular structure of $[Mo(\eta^5\text{-}C_5H_5)_2(o\text{-phen})][PF_6]_2$ (**2**) with 30% probability thermal ellipsoids showing the atom-labeling scheme (only cation illustrated).

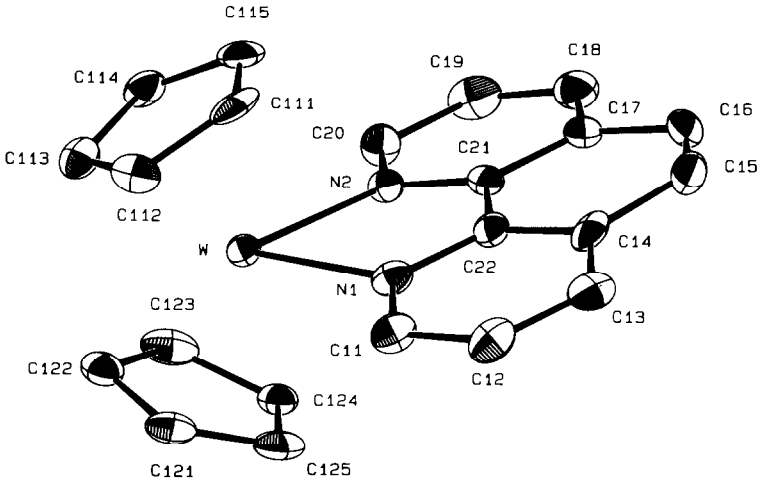

Fig. 4. Molecular structure of $[W(\eta^5\text{-}C_5H_5)_2(o\text{-phen})][PF_6]_2$ (**3**) with 30% probability thermal ellipsoids showing the atom-labeling scheme (only cation illustrated).

character in the Nb–N bonds.

The Mo–N bonding distances in **2**, 2.193(7) and 2.186(7) Å, are in the range of other Mo–N distances observed in biscyclopentadienylmolybdenum complexes with nitrogen donors (see Table 5 in Ref. 17 and Table 5 in Ref. 18).

The W–N bonding distances in **3**, 2.181(11) and 2.179(9) Å, are very similar to the Mo–N bonding distances in **2**. This is not surprising because the two structures are isostructural.

Table 2

Bond lengths (Å) and bond angles (°) for $[Cp_2Nb(bpy)][PF_6]_2$

N(1)–Nb	2.226(6)	N(2)–Nb	2.218(6)
C(11)–N(1)	1.354(8)	C(15)–N(1)	1.339(8)
C(12)–C(11)	1.383(9)	C(16)–C(11)	1.470(9)
C(13)–C(12)	1.373(11)	C(14)–C(13)	1.361(12)
C(15)–C(14)	1.377(10)	C(16)–N(2)	1.342(8)
C(20)–N(2)	1.346(8)	C(17)–C(16)	1.384(9)
C(18)–C(17)	1.371(11)	C(19)–C(18)	1.360(12)
C(20)–C(19)	1.372(11)		
Cp(1)–Nb	2.067(9)		
Cp(2)–Nb	2.067(10)		
N(2)–Nb–N(1)	72.6(3)	Cp–Nb–Cp	133.1(3)
C(11)–N(1)–Nb	117.5(5)	C(15)–N(1)–Nb	122.8(5)
C(15)–N(1)–C(11)	119.5(6)	C(12)–C(11)–N(1)	120.8(7)
C(16)–C(11)–N(1)	115.4(6)	C(16)–C(11)–C(12)	123.7(7)
C(13)–C(12)–C(11)	119.0(8)	C(14)–C(13)–C(12)	119.9(7)
C(15)–C(14)–C(13)	119.3(8)	C(14)–C(15)–N(1)	121.4(7)
C(16)–N(2)–Nb	118.3(5)	C(20)–N(2)–Nb	122.7(5)
C(20)–N(2)–C(16)	119.0(6)	N(2)–C(16)–C(11)	115.6(6)
C(17)–C(16)–C(11)	123.3(7)	C(17)–C(16)–N(2)	121.1(7)
C(18)–C(17)–C(16)	118.9(8)	C(19)–C(18)–C(17)	120.2(8)
C(20)–C(19)–C(18)	118.8(8)	C(19)–C(20)–N(2)	122.0(8)

Table 3

Bond lengths (Å) and bond angles (°) for $[Cp_2Mo(o\text{-phen})][PF_6]_2$

N(1)–Mo	2.193(7)	N(2)–Mo	2.186(7)
C(11)–N(1)	1.329(10)	C(22)–N(1)	1.359(10)
C(20)–N(2)	1.332(10)	C(21)–N(2)	1.349(10)
C(12)–C(11)	1.390(12)	C(13)–C(12)	1.362(14)
C(14)–C(13)	1.405(13)	C(15)–C(14)	1.429(13)
C(22)–C(14)	1.407(11)	C(16)–C(15)	1.339(14)
C(17)–C(16)	1.449(12)	C(18)–C(17)	1.389(13)
C(21)–C(17)	1.404(11)	C(19)–C(18)	1.342(13)
C(20)–C(19)	1.384(12)	C(22)–C(21)	1.417(11)
Cp(1)–Mo	1.969(10)	Cp(2)–Mo	1.976(10)
N(2)–Mo–N(1)	74.7(3)	Cp–Mo–Cp	131.3(4)
C(11)–N(1)–Mo	126.1(6)	C(22)–N(1)–Mo	114.6(5)
C(22)–N(1)–C(11)	119.2(7)	C(20)–N(2)–Mo	125.7(6)
C(21)–N(2)–Mo	115.2(5)	C(21)–N(2)–C(20)	119.0(7)
C(22)–C(11)–N(1)	121.6(9)	C(13)–C(12)–C(11)	120.4(9)
C(14)–C(13)–C(12)	119.2 (9)	C(15)–C(14)–C(13)	124.6(9)
C(22)–C(14)–C(13)	117.5(8)	C(22)–C(14)–C(15)	117.8(9)
C(16)–C(15)–C(14)	121.5(9)	C(17)–C(16)–C(15)	121.8(9)
C(18)–C(17)–C(16)	125.5(9)	C(21)–C(17)–C(16)	117.5(8)
C(21)–C(17)–C(18)	117.0(8)	C(19)–C(18)–C(17)	119.9(8)
C(17)–C(21)–N(2)	122.3(8)	C(19)–C(20)–N(2)	120.9(9)
C(22)–C(21)–N(2)	117.4(7)	C(22)–C(21)–C(17)	120.3(8)
C(14)–C(22)–N(1)	121.9(8)	C(21)–C(22)–N(1)	117.1(7)
C(21)–C(22)–C(14)	121.0(8)		

To our knowledge, the only other biscyclopentadienyl-tungsten complex with a comparable W–N bond length is $[WCp_2(H_2NNPh)][BF_4]$ [19]. One W–N bond in this complex is a typical single W–N bond, 2.156(9) Å, while the other is shorter, 2.034(9) Å, due to some back donation from the metal atom. In $[WCp_2H(p\text{-}NNHC_6H_4F][PF_6]$ the W–N separation of 1.837(7) Å was considered to indicate significant multiple-bond character [20].

The N–M–N bonding angles in **1**, **2** and **3**, 72.6(3)° for Nb, 74.7(3)° for Mo, and 74.7(4)° for W, confirm what has already been observed in many structures of biscyclopentadienyl complexes [17,18], namely that the value of this angle is mainly determined by the steric requirements imposed on the metal by a rigid bidentate ligand. The value of that angle is the same for the two d^2 Mo and W complexes with *o*-phen and very similar to that of the d^1 Nb complex with bipyridine. In all three cases the values differ from the theoretical value predicted from EHMO calculations [21] for a model dihydride derivative, 78° for d^2 and 85° for d^1 complexes.

When three-membered rings are formed, the L–M–L angle is necessarily small e.g., 32.0(2)° in $[MoCp_2(NCCH_3)]$ [22] and 39.7(3)° in $[WCp_2(H_2NNPh)][BF_4]$ [19]. Ligands forming four-membered rings lead to more open angles, e.g., $[MoCp_2(2\text{-}ONC_5H_4)][PF_6]$ and $[MoCp_2(2\text{-}NHNC_5H_4)][PF_6]$ [17], with angles of 61.2(4) and 59.8(1)°, respectively, and $[MoCp_2(SO_4)]$ [23] with an angle of 66.1(2)°. Five-membered rings, e.g., as in $[MoCp_2(N_2C_3H_3C(CH_3)_2O)][PF_6]$ [24], 75.4(1)°, have angles similar to those found in the title complexes.. The L–M–L angles between *cis* monodentate ligands are comparable to those theoretically predicted,

Table 4

Bond lengths (Å) and bond angles (°) for $[Cp_2W(o\text{-phen})][PF_6]_2$

N(1)–W	2.181(11)	N(2)–W	2.179(9)
C(11)–N(1)	1.332(13)	C(22)–N(1)	1.374(13)
C(20)–N(2)	1.321(13)	C(21)–N(2)	1.355(13)
C(12)–C(11)	1.380(17)	C(13)–C(12)	1.376(17)
C(14)–C(13)	1.404(17)	C(15)–C(14)	1.457(18)
C(22)–C(14)	1.385(15)	C(16)–C(15)	1.392(21)
C(17)–C(16)	1.427(17)	C(18)–C(17)	1.410(17)
C(21)–C(17)	1.398(15)	C(19)–C(18)	1.367(21)
C(20)–C(19)	1.387(17)	C(22)–C(21)	1.416(15)
Cp(1)–W	1.960(12)	Cp(2)–W	1.969(13)
N(2)–W–N(1)	74.7(4)	Cp–W–Cp	130.2(5)
C(11)–N(1)–W	125.7(8)	C(22)–N(1)–W	115.6(7)
C(22)–N(1)–C(11)	118.6(1.0)	C(20)–N(2)–W	125.9(0.7)
C(21)–N(2)–W	115.0(0.6)	C(21)–N(2)–C(20)	118.9(0.8)
C(12)–C(11)–N(1)	120.8(1.1)	C(13)–C(12)–C(11)	122.3(1.1)
C(14)–C(13)–C(12)	117.2(1.1)	C(15)–C(14)–C(13)	123.4(1.1)
C(22)–C(14)–C(13)	118.6(1.1)	C(22)–C(14)–C(15)	118.0(1.1)
C(16)–C(15)–C(14)	119.8(1.1)	C(17)–C(16)–C(15)	120.6(1.1)
C(18)–C(17)–C(16)	122.1(1.1)	C(21)–C(17)–C(16)	119.5(1.1)
C(21)–C(17)–C(18)	118.4(1.1)	C(19)–C(18)–C(17)	117.6(1.0)
C(20)–C(19)–C(18)	121.1(1.1)	C(19)–C(20)–N(2)	121.9(1.1)
C(17)–C(21)–N(2)	122.2(0.9)	C(22)–C(21)–N(2)	118.1(0.9)
C(22)–C(21)–C(17)	119.7(0.9)	C(14)–C(22)–N(1)	122.4(1.0)
C(21)–C(22)–N(1)	115.5(0.9)	C(21)–C(22)–C(14)	122.0(0.9)

e.g., 83.8(2)° in $[NbCp_2(NCCH_3)_2][BF_4]_2$ [13] and 79.8(1)° in $[MoCp_2(SPh)(p\text{-}(CH_3)_2N\text{-}C_6H_4CN)][PF_6]$ [18].

Comparison of the M–N distances and the N–M–N angles with those of other Nb, Mo, and W complexes containing coordinated bipyridine or *o*-phenanthroline would be interesting but no examples of Nb or W complexes were found in the literature. The overall geometry of these coordinated ligands is similar in all cases, except for $[Mo(O^iPr)_2(bpy)_2]$, as will be discussed later. Table 5 lists Mo–N distances and N–Mo–N angles in Mo complexes.

The bond distances and bond angles in the coordinated bipyridine ligand in **1** and in the *o*-phenanthroline ligand in **2** and **3** are normal and comparable to the corresponding values for the examples quoted in Table 5 and also with the values observed in the free ligands [33,40]. The bipyridine in **1** is planar with maximum deviations from planarity of 0.069(8) Å, while the *o*-phenanthrolines in **2** and **3** are less planar with maximum deviations of 0.12(1) and 0.11(1) Å, respectively.

Molecular orbital calculations

Extended Hückel molecular-orbital calculations were done on the model compounds $[MoCp_2(o\text{-phen})]^{2+}$ and $[MoCp_2(bpy)]^{2+}$. A molecular orbital diagram depicting the interaction between the $MoCp_2$ fragment and bpy is shown in Fig. 5.

The frontier orbitals of the metallic fragment [21] are represented on the left side. The bpy σ bonds correspond to the interactions between the symmetric combination of the two nitrogen lone pairs and $2a_1$, and the antisymmetric combination and b_2. 0.30 electrons are transferred from the ligand to $2a_1$ and 0.44

Table 5

Comparison of molecular parameters in Mo complexes with bipyridine and *o*-phenanthroline ligands [25]

Formula	Oxidation state	$d\langle$Mo–N$\rangle$ (Å)	N–Mo–N (°)	Reference
$[Mo(O)_2(CH_3)_2(bpy)]$	VI	2.330(2)	68.4(6)	26
$[Mo(O)_2(C_2H_5)_2(bpy)]$	VI	2.326(6)	69.0(2)	27
$[Mo(O)_2(4\text{-}CH_3OC_6H_4)_2(bpy)]$	VI	2.317(2)	68.92(9)	28
$[Mo(O)_2[CH_2C(CH_3)_3]_2(bpy)]$	VI	2.333(4)	68.6(1)	29
$[Mo(O)_2(CH_2C_6H_5)_2(bpy)]$	VI	2.29(1)	69.9(5)	30
$[Mo(CO)_3(bpy)(dipyam)]$	0	2.246(6)	72.2(2)	31
$[Mo(CO)_2(\eta^3\text{-}CH_2C(CONHMe)(C{=}CH_2)(bpy)(O_2CC_3F_7)]$	I	2.256(8)	74.0(3)	32
$[Mo(O^iPr)_2(bpy)_2]$	II	2.115(2)	73.9(1)	33
		2.120(2)	73.3(1)	33
$[\mu\text{-}Cl\{Mo(bpy)(CO)_2(\eta^3\text{-}C_3H_5)\}_2]^+$	II	2.255(8)	72.6(3)	34
$[Mo(CN^tBu)_3(^tBuHNC)_2(bpy)]^{2+}$	II	2.22(2)	72.6(6)	35
		2.23(2)	72.7(4)	35
$[Mo(NO)_2(bpy)Cl_2]$	IV	2.198(7)	74.3(4)	36
$[Mo(CO)_2(NCCH_3)(\eta^3\text{-allyl})(bpy)]^+$	II	2.243(7)	72.0(3)	37
$MoO(CN)_3(o\text{-phen})]^-$	IV	2.268(7)	71.6(3)	38
	IV	2.269(7)	71.0(2)	39
$[MoCp_2(o\text{-phen})]^+$	IV	2.190(7)	74.7(3)	this work

to b_2. No back donation from the metal to the ligand is suggested. This can be inferred in several ways. The empty π^* orbitals of bpy do not overlap significantly with any of the $MoCp_2$ orbitals, and are unperturbed. A possible reason is that the

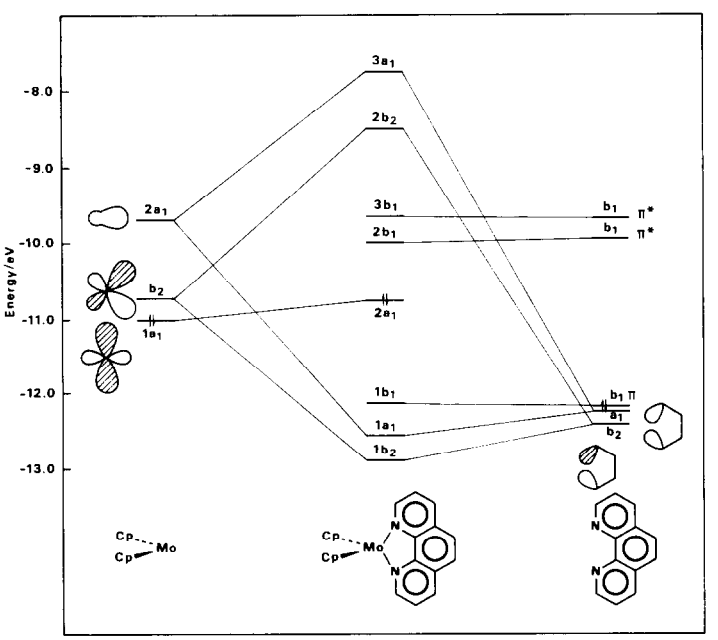

Fig. 5. Interaction diagram between the $MoCp_2$ fragment and *o*-phenanthroline.

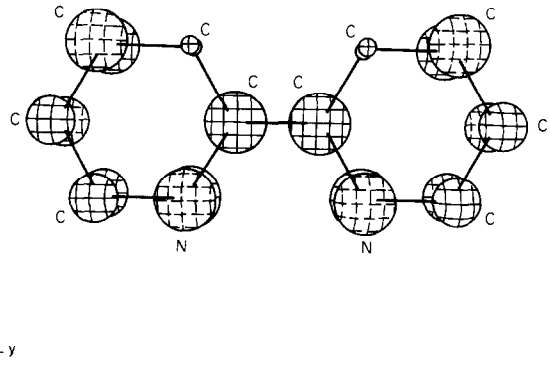

Fig. 6. The LUMO of bipyridine.

π^* orbitals have a nodal plane in yz, where the donor orbitals are mostly localized. The $1a_1$ orbital of the $MoCp_2$ fragment remains almost non-bonding. If Nb^{IV} rather than Mo^{IV} is considered, the only qualitative difference is that only one electron occupies the HOMO, which is metal-centred. This should lead to a different redox behaviour. On the other hand, the fact that only a σ interaction takes place between Mo and bpy and that the π^* orbitals of the ligand are not involved, implies that no significant changes on bond lengths should occur. We can consider, for instance, the central C–C bond of bpy. Its lowest π^* orbital of bpy shown in Fig. 6 is strongly bonding between these two carbon atoms.

Back donation from the metal should strengthen this bond and lead to a shorter C–C distance, as well as to stronger M–N bonds. Table 6 gives both these C–C and M–N distances and their respective calculated overlap populations for free bipyridine, $[NbCp_2(bpy)]^{2+}$, the model $[MoCp_2(bpy)]^{2+}$, and $[Mo(O^iPr)_2(bpy)_2]$ [33]. The overlap populations were obtained for the same bond lengths inside bpy. A higher overlap population means that the bond is stronger and the real distance should be shorter. The calculated values point in the right direction. Small increases of C–C overlap population for the MCp_2 derivatives result in the slightly shorter C–C bond observed in $[NbCp_2(bpy)]^{2+}$; on the other hand, the larger increase for $[Mo(O^iPr)_2(bpy)_2]$ is reflected in the much shorter bond [33]. The interaction diagram for this complex (not shown) includes a strong interaction between empty bpy π^* and a filled Mo d orbital. This multiple bond character of the Mo–N bonds shows up in their lengths (2.115, 2.120 Å). These are shorter than

Table 6

Distances and overlap populations in complexes with bpy

Complex	d(C–C) (Å)	Overlap population	$d\langle$M–N$\rangle$ (Å)	Overlap population
Free bpy	1.490	0.967		
$[NbCp_2(bpy)]^{2+}$	1.474	0.987	2.226	0.473
$[MoCp_2(bpy)]^{2+}$	–	0.988	–	0.400
$[Mo(O^iPr)_2(bpy)_2]$	1.425	1.019	2.115	0.459
	1.424	1.019	2.120	0.453

all the others in Table 5, which appear in complexes where back donation is not expected (either the metal is in a high formal oxidation state, or there is strong competition from stronger π acceptor ligands, such as CO, in the formally Mo^{II} compounds). For the *o*-phenanthroline complexes the central C–C bond belongs to a benzene ring and the observation of this change is not so clear. On the other hand, no system was found where back donation might be important.

Conclusions

The dicationic Nb^{IV} complexes containing bypiridine or *o*-phenanthroline exhibit a redox behaviour different from that of the known neutral Nb^{IV} species, and the ligand is also easily reduced, and at less negative potentials than when free. The absence of back donation from the metal as seen from the molecular orbital diagram, is in agreement with the experimental electrochemical data, and with the observed bond lengths in the complexes, which show no significant difference from those of the uncoordinated ligand.

Experimental

All preparations were carried out under a dry nitrogen atmosphere or in vacuum by the usual Schlenk techniques. The solvents were reagent grade materials. They were dried by standard methods [41] and distilled just before use under argon atmosphere. The starting materials $[MCp_2X_2]$ were prepared by reported methods M = Nb, X = Cl [42], M = Mo, W; X = I [43]. Complexes $[MoCp_2(o\text{-phen})][PF_6]_2$ and $[WCp_2(o\text{-phen})][PF_6]_2$ were prepared following the published procedure [1].

Preparation of $[NbCp_2(bpy)][PF_6]$

The complex $[NbCp_2Cl_2]$ (300 mg, 1 mmol), $TlPF_6$ (1.1 g, *ca.* 3 mmol) and bipyridine (160 mg, *ca.* 1 mmol) were stirred in 1,2-dibromoethane at room temperature for 5 h. After filtration of thallium chloride, the solvent was evaporated under vacuum, and the red-orange solid residue was recrystallized from acetonitrile/ether. Crystals for X-ray structural determinations were grown from a concentrated solution of the compound in acetonitrile which was kept in a deep freeze, after adding a few drops of diethyl ether.

Electrochemical apparatus

The electrochemistry instrumentation consisted of a Princeton Applied Research model 173 potentiometer, model 175 voltage programmer, model 179 digital coulometer and an Omnigraphic 2000 X-T recorder of Houston Instruments. Potentials were referred to a calomel electrode (SCE) containing a saturated solution of potassium chloride checked relative to a 1.0×10^{-3} *M* solution of ferrocene in acetonitrile containing 0.10 *M* $LiClO_4$, for which the ferrocinium/ferrocene potential was in agreement with the literature [44]. The working electrode was made of a 2-mm piece of Pt wire. The secondary electrode was a Pt wire coil. The experiments were performed in a PAR polarographic cell, at room temperature, with solutions 1 m*M* in solute and 0.1 *M* in the supporting electrolyte, tetrabutylammonium hexafluorophosphate. The solvent CH_3CN was re-

Table 7

Experimental details for the crystallographic analysis

	1	2	3
Formula	$C_{20}H_{18}N_2P_2F_{12}Nb$	$C_{22}H_{18}N_2P_2F_{12}Mo$	$C_{22}H_{18}N_2P_2F_{12}W$
M	669.21	696.3	784.2
Crystal system	monoclinic	monoclinic	monoclinic
Space group	$P2_1/c$	$P2_1/n$	$P2_1/n$
Unit cell determination	25 automatically centred reflections with $12 \leq \theta \leq 18°$	25 automatically centred reflections with $12 \leq \theta \leq 15°$	
a (Å)	10.729(1)	12.339(1)	12.305(3)
b (Å)	15.10(1)	14.138(2)	14.152(7)
c (Å)	14.630(2)	13.743(3)	13.760(6)
β (°)	90.58(2)	100.38(2)	100.33(1)
V (Å^3)	2370.96	2358.26	2357.31
Z	4	4	4
D_c (g cm^{-3})	1.87	1.96	2.21
μ(Mo-K_α) (cm^{-1})	6.78	7.05	52.0
Diffractometer	CAD4	CAD4	Fast
Radiation	Mo-K_α (λ 0.71069 Å)	Mo-K_α	Mo-K_α
Scan range (°)	$2.0 \leq \theta \leq 27.0$	$1.5 \leq \theta \leq 25.0$	$0 \leq \theta \leq 31$
Scan type	$\omega-2\theta$	$\omega-2\theta$	
Nr. of unique data	4562	3681	6305
Nr. of data with $F \geq 3\sigma(F)$	3644	2831	3755
Decay during data collection	none	none	none
Largest shift/error on final cycle	0.006	0.048	0.127
Largest peak in final Diff. Fourier (e/Å^3)	0.833	0.698	0.339
R [a]	0.050	0.045	0.050
R_w [b]	0.050	0.045	0.057
Nr. of parameters	406	409	355
Weighting scheme	unit	unit	$0.0901/(\sigma^2(F)+0.032265(F)^2)$

[a] $R = \Sigma(F_o - F_c)/\Sigma F_o$. [b] $R_w = \Sigma(F_o - F_c)w^{1/2}/\Sigma(F_o w^{1/2})$.

fluxed for several hours over CaH_2 and P_2O_5 and distilled under dry nitrogen just before use. Solutions were degassed with dry nitrogen before each experiment and a nitrogen atmosphere was always maintained over the solution.

Data collection

The pertinent crystallographic parameters for complexes **1**, **2** and **3** are given in Table 7.

Intensity data were collected for complexes **1** and **2** on a Enraf–Nonius CAD-4 diffractometer with graphite-monochromatized radiation. The data were corrected for absorption, Lorentz and polarization effects with the CAD-4 software. Cell dimensions were determined from 25 intense reflections automatically centred with $1.2 < \theta < 18°$ for **1** and $1.2 < \theta < 15°$ for **2**.

Intensity data for complex **3** were collected on a FAST area detector diffractometer with a FR571 rotating anode generator, operating at 3.0 kW, equipped with a molybdenum rotating anode (λ 0.71069 Å) and graphite monochromator.

Table 8

Fractional atomic coordinates ($\times 10^4$) for $[Cp_2Nb(bpy)][PF_6]_2$

Atom	x	y	z
Nb	1872.6(4)	600.4(3)	2026.3(3)
N(1)	2566(4)	925(3)	3426(3)
C(11)	3755(5)	1216(4)	3511(4)
C(12)	4292(7)	1347(5)	4363(5)
C(13)	3604(8)	1169(5)	5128(5)
C(14)	2403(8)	890(5)	5039(5)
C(15)	1899(6)	772(4)	4178(4)
N(2)	3743(4)	1207(3)	1884(3)
C(16)	4389(5)	1408(4)	2647(4)
C(17)	5571(6)	1770(5)	2605(6)
C(18)	6079(7)	1931(5)	1765(6)
C(19)	5427(7)	1732(5)	989(6)
C(20)	4260(6)	1370(5)	1066(5)
C(111)	−175(6)	1195(6)	2140(6)
C(112)	626(7)	1894(5)	2359(5)
C(113)	1331(7)	2084(5)	1593(5)
C(114)	966(7)	1519(5)	893(5)
C(115)	16(7)	971(6)	1228(6)
C(121)	1059(8)	−792(5)	1544(8)
C(122)	2088(9)	−635(5)	1035(5)
C(123)	3093(8)	−654(6)	1622(10)
C(124)	2651(15)	−799(5)	2502(9)
C(125)	1395(13)	−883(5)	2431(7)
P(1)	3010(2)	959(1)	8241(1)
F(11)	1912(5)	759(5)	7577(4)
F(12)	2236(7)	1728(5)	8672(5)
F(13)	3826(7)	250(5)	7802(5)
F(14)	4094(5)	1193(6)	8905(4)
F(15)	3533(7)	1616(4)	7517(4)
F(16)	2428(8)	365(6)	8987(5)
P(2)	8395(2)	1766(1)	4812(1)
F(21)	7227(4)	1280(3)	5265(3)
F(22)	9564(4)	2242(3)	4378(3)
F(23)	8405(5)	2458(5)	5597(4)
F(24)	9276(5)	1156(5)	5375(5)
F(25)	7463(6)	2358(4)	4267(5)
F(26)	8374(8)	1062(4)	4037(4)

A crystal-to-detector distance of 40 mm and a swing angle of $\theta = 25°$ were used. The exposure time was 15 s per frame and an increment between frames of 0.15°. At $\chi = 0°$, one scan of 100° through ω was done, followed by a second 100° scan with ϕ shifted 90° from the previous position. The missing data were then recorded by making three 90° ω scans at $\chi = 45°$, 45° apart in ϕ; and three final 70° ω scans at $\chi = 90°$, again 45° apart in ϕ.

The data were evaluated on-line using the modified MADNES [45] software for small molecules, SADNES. With this procedure, a total of 37262 reflections were measured, which reduced to 6305 unique.

The initial values of the cell parameters were determined by an autoindexing procedure applied to 50 intense reflections covering two narrow (*ca.* 5° wide) and nearly orthogonal regions of reciprocal space. Throughout the data collection

Table 9
Fractional atomic coordinates ($\times 10^4$) for $[Cp_2Mo(o\text{-phen})][PF_6]_2$

Atom	x	y	z
Mo	310.4(5)	2436.6(4)	2464.4(4)
N(1)	570(5)	3956(4)	2731(4)
N(2)	537(4)	2605(4)	4069(4)
C(11)	502(7)	4624(5)	2043(6)
C(12)	739(7)	5565(6)	2288(8)
C(13)	1085(7)	5823(6)	3248(8)
C(14)	1174(6)	5130(5)	3992(6)
C(15)	1508(7)	5313(7)	5025(8)
C(16)	1497(7)	4632(7)	5701(7)
C(17)	1130(6)	3680(6)	5422(6)
C(18)	1018(7)	2952(7)	6075(6)
C(19)	694(8)	2092(7)	5725(6)
C(20)	458(6)	1920(6)	4717(6)
C(21)	850(5)	3476(5)	4409(5)
C(22)	879(6)	4198(5)	3698(5)
C(111)	1204(7)	1382(6)	1646(6)
C(112)	1522(7)	2291(6)	1383(6)
C(113)	2138(6)	2686(6)	2222(7)
C(114)	2138(6)	2061(7)	3008(6)
C(115)	1561(7)	1244(6)	2666(7)
C(121)	−1158(6)	2628(7)	1192(6)
C(122)	−1489(7)	3060(6)	2008(7)
C(123)	−1514(6)	2363(7)	2745(6)
C(124)	−1211(7)	1491(6)	2387(7)
C(125)	−1017(6)	1656(6)	1422(7)
P(1)	163(2)	1365(2)	8509(2)
F(11)	10608(6)	618(5)	9339(4)
F(12)	10328(9)	621(5)	7727(5)
F(13)	11306(6)	1765(6)	8517(8)
F(14)	9886(8)	2081(5)	9282(5)
F(15)	8965(6)	951(5)	8486(7)
F(16)	9651(5)	2087(4)	7667(4)
P(2)	2422(2)	4535(2)	9764(2)
F(21)	3617(6)	4817(5)	9668(7)
F(22)	2735(5)	3467(4)	9637(4)
F(23)	2729(6)	4431(4)	10916(4)
F(24)	2142(7)	5613(4)	9903(5)
F(25)	2047(6)	4643(5)	8595(4)
F(26)	1209(5)	4228(6)	9827(5)

process, the cell parameters were refined together with the orientation matrix every 9° of measured data. The values used in the structure determination and refinement are the mean and corresponding standard deviations calculated from the refined values of the cell parameters which were based on more than 200 intense reflections.

Data reduction including Lorentz and polarization corrections was carried out by the Kabsch profile fitting method using the program PROCOR [46]. The data were then scaled and merged with the program SHELX76 [47], givin an R_{merge} of 9% $\left(R_{merge} = \sqrt{\sum_i N_i \sum_j \left[\left(1/\sigma_{ij}^2\right)\left(F_{ij} - \langle F_i \rangle\right)^2\right] / \sum_i \left[\left(N_i - 1\right)\sum_j \left(F_{ij}^2/\sigma_{ij}^2\right)\right]}\right)$.

Table 10

Fractional atomic coordinates ($\times 10^4$) for $[Cp_2W(o\text{-phen})][PF_6]_2$

Atom	x	y	z
W	304.2(3)	2429.3(2)	2457.0(3)
N(1)	570(7)	3939(6)	2716(6)
N(2)	519(7)	2604(5)	4054(5)
C(11)	501(9)	4602(8)	2021(8)
C(12)	747(10)	5532(8)	2268(9)
C(13)	1077(8)	5820(8)	3230(9)
C(14)	1174(8)	5121(8)	3965(9)
C(15)	1532(10)	5318(10)	5013(10)
C(16)	1467(9)	4613(10)	5707(10)
C(17)	1115(8)	3683(8)	5399(8)
C(18)	1026(9)	2956(10)	6080(9)
C(19)	676(10)	2090(10)	5710(9)
C(20)	441(9)	1929(8)	4700(8)
C(21)	852(7)	3476(7)	4390(7)
C(22)	879(7)	4203(7)	3687(7)
C(111)	2152(9)	2704(8)	2244(11)
C(112)	1517(9)	2300(8)	1390(8)
C(113)	1177(8)	1372(8)	1646(7)
C(114)	1533(9)	1221(8)	2642(7)
C(115)	2167(8)	2046(10)	3017(9)
C(121)	−1178(10)	2630(8)	1195(9)
C(122)	−1018(8)	1647(8)	1413(8)
C(123)	−1203(8)	1487(9)	2393(9)
C(124)	−1537(8)	2384(7)	2745(8)
C(125)	−1499(8)	3061(10)	2043(9)
P(1)	2423(3)	4541(2)	9772(2)
F(11)	3629(7)	4835(8)	9733(10)
F(12)	1200(7)	4229(9)	9808(8)
F(13)	2131(9)	5607(7)	9925(7)
F(14)	2739(7)	3482(5)	9636(7)
F(15)	2708(8)	4413(7)	10915(5)
F(16)	2065(8)	4672(8)	8620(6)
P(2)	181(3)	1359(2)	8516(2)
F(21)	1313(8)	1770(10)	8565(12)
F(22)	611(8)	604(8)	9329(6)
F(23)	−117(12)	2071(10)	9307(7)
F(24)	403(13)	639(9)	7722(7)
F(25)	−309(8)	2105(7)	7683(6)
F(26)	−1027(9)	931(9)	8470(10)

Structure determination and refinement

The heavy atom positions were located in each case from a Patterson map and the remaining non-hydrogen positions from subsequent difference Fourier maps. In the case of complex **3** an absorption correction was applied with the program DIFABS [48] after the isotropic refinement, improving the R factor from 0.083 to 0.064. Least-squares refinement was continued with anisotropic thermal parameters for all non-H atoms.

The hydrogen atoms for compound **1** were all located in a difference map and refined individually, while for compounds **2** and **3** these atoms were included in the calculated positions and refined in three groups according to the ligand they

Table 11

Orbitals and parameters for the extended Hückel calculations

Orbital	$-H_{ii}$ (eV)	ζ_1	ζ_2	C_1	C_2
Nb 5*s*	10.10	1.889			
Nb 5*p*	6.86	1.852			
Nb 4*d*	12.10	4.08	1.63	0.6583	0.5673
Mo 5*s*	8.77	1.96			
Mo 5*p*	5.60	1.90			
Mo 4*d*	11.06	4.54	1.90	0.5899	0.5899

belong to, with one general temperature factor for each group. A weighting scheme was necessary in the refinement of complex **3** before final convergence. Final values for the three complexes are listed in Table 7.

Final atomic coordinates are given in Tables 8, 9 and 10 for complexes **1**, **2** and **3** respectively. The atomic coordinates and thermal parameters for the H atoms, anisotropic thermal parameters for all non-H atoms and lists of observed and calculated structure factors are available from the authors.

The computations required to solve and refine the structures were done using programs SHELX86 [49] and SHELX76 [47]. Drawings were made with the program ORTEP-II [50]. Atomic scattering values were taken from International Tables [51].

Molecular orbital calculations

All calculations were of the extended Hückel type [5] with modified H_{ij}'s [52]. The basis set for the metal atoms consisted of *ns*, *np* and $(n-1)d$ orbitals. The *s* and *p* orbitals were described by single Slater-type wave functions, and the *d* orbitals were taken as contracted linear combinations of two Slater-type wave functions.

The geometries of $[MCp_2(L\text{–}L)]^{2+}$ (L–L = bpy or *o*-phen) were taken from those described in this work and $[Mo(OH)_2(bpy)_2]$ was a model for $[Mo(O^iPr)_2(bpy)_2]$ [33]. Typical distances (Å) and angles (°) are: M–Cp 2.00, M–N 2.19, C–C = C–N 1.40, C–H 1.08, Cp–M–Cp 132.

Standard parameters were used for C, N, and H, while those for Mo and Nb are listed in Table 11. The three-dimensional plot of Fig. 6 was made using the program CACAO [53].

Acknowledgements

A. Bram and P.N. Olsen were Erasmus students at I.S.T., Lisbon. Financial support for this work was partially provided by Instituto Nacional de Investigação Científica and Junta Nacional de Investigação Científica e Tecnológica (PMCT/C/CEN/367/90).

We gratefully acknowledge Dr. Fernanda Carvalho at I.S.T. for helpful discussions on the electrochemistry results.

References

1 (a) M.J. Calhorda and A.R. Dias, Rev. Port. Quim., 20 (1978) 77; (b) M.J. Calhorda and A.R. Dias, J. Chem. Soc., Dalton Trans., (1980) 1443.

2 F.J.S. Pina, Doctoral Thesis, Instituto Superior Técnico, Lisbon, 1982.
3 T. Avilez, A.R. Dias, M.L.H. Green and C.C. Romão, J. Chem. Soc., Dalton Trans., (1979) 1367.
4 (a) S.M.B. Costa, A.R. Dias and F.J.S. Pina, J. Organomet. Chem., 175 (1979) 193; (b) S.M.B. Costa, A.R. Dias and F.J.S. Pina, J. Organomet. Chem., 217 (1981) 357; (c) S.M.B. Costa, A.R. Dias and F.J.S. Pina, J. Chem. Soc., Dalton Trans., (1981) 314.
5 (a) R. Hoffmann, J. Chem. Phys., 39 (1963), 1397; (b) R. Hoffmann and W.N. Lipscomb, J. Chem. Phys., 39 (1962) 2179.
6 M.F. Lappert, C.L. Raston, B.W. Skelton and A.H. White, J. Chem. Soc., Dalton Trans., (1984) 893.
7 T. Sagi and S. Aoyagui, J. Electroanal. Chem., 63 (1975) 405.
8 A.A. Vlcek, Coord. Chem. Rev., 43 (1982) 39.
9 J.C. Kotz, W. Vining, W. Coco, R. Rosen, A.R. Dias and M.H. Garcia, Organometallics, 2 (1983) 68.
10 M. Rute Gomes da Costa, Doctoral Thesis, Instituto Superior Técnico, Lisbon, 1986.
11 (a) R.S. Threlkel and J.E. Bercaw, J. Am. Chem. Soc., 103 (1981) 2650; (b) S.I. Bailey, L.M. Engelhardt, W.-P. Leung, C.L. Raston, I.M. Ritchie and A.H. White, J. Chem. Soc., Dalton Trans., (1985) 1747; (c) J.A. Hunter, W.E. Lindsell, K.J. McCullough, R.A. Parr and M.L. Scholes, J. Chem. Soc., Dalton Trans., (1990) 2145.
12 L. Roullier, D. Lucas, Y. Mugnier, A. Antiñolo, M. Fajardo and A. Otero, J. Organomet. Chem., 396 (1990) C12.
13 M.A.A.F. de C.T. Carrondo, J. Morais, C.C. Romão, M.J. Romão and L.F. Veiros, XVth Congress and General Assembly of IUG, Bordeaux, 1990.
14 (a) J. Arnolt, T.D. Tilley, A.L. Rheingold and S.J. Geib, Organometallics, 6 (1987) 473; (b) A. Fakhr, Y. Mugnier, R. Broussier and B. Gautheron, J. Organomet. Chem., 279 (1985) C15; (c) M. Gomez, J.M. Martinez de Ilarduya and P. Royo, J. Organomet. Chem., 369 (1989) 197.
15 A. Antiñolo, P. Gómez-Sal, J.M. Ilarduya, A. Otero, P. Royo, S.M. Carreras and S.G. Blanco, J. Chem. Soc., Dalton Trans., (1987) 975.
16 D.A. Lemenovskii, V.P. Fedin, Yu. L. Slovohotov and Yu. T. Struchkov, J. Organomet. Chem., 228 (1982) 153.
17 M.J. Calhorda, M.A.A.F. de C.T. Carrondo, R.G. Costa, A.R. Dias, M.T.L.S. Duarte and M.B. Hursthouse, J. Organomet. Chem., 320 (1987) 53.
18 M.A.A.F. de C.T. Carrondo, A.R. Dias, M.H. Garcia, P.M. Matias, M.P. Robalo, M.L.H. Green, J. Higgins and Y.Y. Yang, J. Organomet. Chem., 395 (1990) 279.
19 M. Cowie and M.D. Gauthier, Inorg. Chem., 19 (1980) 3142.
20 F.W.B. Einstein, T. Jones, A.J. Lee Hanlan and D. Sutton, Inorg. Chem, 21 (1982) 2589.
21 J.W. Lauher and R. Hoffmann, J. Am. Chem. Soc., 98 (1976) 1729.
22 T.C. Wright, G. Wilkinson, M. Motevalli and M.B. Hursthouse, J. Chem. Soc., Dalton Trans., (1986) 2017.
23 M.J. Calhorda, M.A.A.F. de C.T. Carrondo, A.R. Dias, A.M.T.S. Domingos, J.A. Martinho Simões and C. Teixeira, Organometallics, 5 (1986) 660.
24 M.A.A.F. de C.T. Carrondo and A.M.T.S. Domingos, J. Organomet. Chem., 253 (1983) 53.
25 F.H. Allen, O. Kennard and R. Taylor, Acc. Chem. Res., 16 (1983) 146.
26 G.N. Schrauzer, L.A. Hughes, N. Strampach, P.R. Robinson and E.O. Schlemper, Organometallics, 1 (1982) 44.
27 G.N. Schrauzer, E.O. Schlemper, N.H. Liu, Q. Wang, K. Rubin, X. Zhang, X. Long and C.S. Chin, Organometallics, 5 (1986) 2452.
28 G.N. Schrauzer, X. Zhang, N.H. Liu and E.O. Schlemper, Organometallics, 7 (1988) 279.
29 G.N. Schrauzer, L.A. Hughes, N. Strampach, F. Ross, D. Ross and E.O. Schlemper, Organometallics, 2 (1983) 481.
30 G.N. Schrauzer, L.A. Hughes, E.O. Schlemper, F. Ross and D. Ross, Organometallics, 2 (1983) 1163.
31 A. Howie and G.P. McQuillan, J. Chem. Soc., Dalton Trans., (1986) 759.
32 B.J. Brisdon, R.J. Deeth, A.G.W. Hodson, C.M. Kemp, M.F. Mahon and K.C. Molloy, Organometallics, 10 (1991) 1107.
33 M.H. Chisholm, J.C. Huffman, I.P. Rothwell, P.G. Bradley, N. Kress and W.H. Woodruff, J. Am. Chem. Soc., 103 (1981) 4945.
34 M.D. Curtis and N.A. Fotinos, J. Organomet. Chem., 272 (1984) 43.
35 S. Warner and S.J. Lippard, Organometallics, 5 (1986) 1716.

36 D.B. Tkatchenko, C. Bremard, F. Abraham and G. Nowogrocki, J. Chem. Soc., Dalton Trans., (1983) 1137.
37 M.A.A.F. de C.T. Carrondo and A.M. Galvão, unpublished results.
38 S.S. Basson, J.G. Leipoldt and I.M. Potgieter, Inorg. Chim. Acta, 90 (1984) 57.
39 S.S. Basson, J.G. Leipoldt and I.M. Potgieter, Inorg. Chim. Acta, 87 (1984) 71.
40 S. Nishigaki, H. Yoshioka and K. Nakatsu, Acta Crystallogr., Sect. B, 34 (1978) 875.
41 D.D. Perrin, W.L.F. Amarego and D.R. Perrin, Purification of Laboratory Chemicals, 2nd ed., Pergamon Press, 1980.
42 A. Van Baalen, C.J. Groenenboom and H.J. de Liefde Meijer, J. Organomet. Chem., 74 (1974) 245.
43 R.L. Cooper and M.L.H. Green, J. Chem. Soc. A, (1967) 1155.
44 I.V. Nelson and R.T. Iwando, Anal. Chem., 35 (1963) 867.
45 A. Messerschmidt and J.W. Pflugrath, J. Appl. Crystallogr., 20 (1987) 306; J.W. Pflugrath and A. Messerschmidt, Crystallography in Molecular Biology, Meeting Abstracts, Bischenberg, France, 1985.
46 W. Kabsch, J. Appl. Crystallogr., 21 (1988) 916.
47 G.M. Sheldrick, SHELX; Crystallographic Calculation Program, University of Cambridge, 1976.
48 N. Walker, D. Stuart, 'DIFABS', An Empirical Method for Correcting Diffractometer Data for Absorption Effects, Acta Crystallogr., Sect. A, 39 (1983) 158.
49 G.M. Sheldrick, in G.M. Sheldrick, C. Krüger and R. Goddard (Eds.), Crystallographic Computing 3, Oxford University Press, 1985.
50 C.K. Johnson, ORTEP-II, Report ORNL-5138, Oak Ridge National Laboratory, Park Ridge, Tennessee, 1976.
51 International Tables for X-Ray Crystallography, Vol. IV, Kynoch Press, Birmingham, UK, 1974.
52 J.H. Ammeter, H.-B. Bürgi, J.C. Thibeault and R. Hoffmann, J. Am. Chem. Soc., 100 (1978) 3686.
53 C. Mealli and D.M. Proserpio, J. Chem. Educ., 66 (1990) 399.